MECHANICAL PROPERTIES AND CORROSION RESISTANCE OF MIM NI-BASED SUPERALLOYS

John L. Johnson, Lye King Tan,* Pavan Suri,** and Randall M. German**

AMTellect, Inc., State College, PA 16801
*Advanced Materials Technologies Pte Ltd, Singapore 609602
**The Pennsylvania State University, University Park, PA 16802

ABSTRACT

Superalloys based on nickel exhibit a combination of strength and resistance to surface degradation that make them useful for many applications. Metal injection molding (MIM) of HX, 718, and 625 is evaluated. Sintering conditions for these alloys are optimized to achieve maximum density and their microstructures are characterized. 718 and 625 achieve high sintered densities via supersolidus liquid phase sintering, but pore-grain boundary break-away occurs for HX before liquid forms so lower sintered densities are achieved. The mechanical properties of MIM 718 and 625 are compared to cast, wrought, and previously reported MIM properties. The corrosion resistance of these materials is tested in various media and compared to 316L stainless steel and commercially pure Ni. While these two materials perform well under oxidizing and reducing conditions respectively, the superalloys, especially 625, perform well in both types of corrosive environments.

INTRODUCTION

Superalloys are a class of heat-resisting alloys based on nickel, nickel-iron, or cobalt that exhibit a combination of strength and resistance to surface degradation at both elevated and cryogenic temperatures. These properties make them useful for many applications in the aerospace, automotive, medical, chemical, and petrochemical industries, but their high strength and toughness make them difficult to shape via machining or forging. Investment casting is often used to process superalloys, but can be costly. An alternative process is metal injection molding (MIM), which enables complex geometry designs, minimum material loss, quick scale-up response time, and significant cost savings on moderate or large production volumes. Current use of MIM superalloys is limited partially due to scarce mechanical property and corrosion resistance data.

Complex valves and fittings for chemical processes provide opportunities for MIM to provide a low-cost, high-volume process that can meet geometry and property requirements. However, a variety of corrosive environments are encountered in the chemical processing industry, requiring different material solutions. Austenitic stainless steels, such as 316L, are commonly available via MIM and are useful for oxidizing conditions, including exposure to nitric acid, phosphoric acid, and concentrated sulfuric acid, since they

maintain corrosion resistance through a passive oxide layer. More reducing conditions break down this layer, making the steel susceptible to pitting and crevice corrosion. Alloys with higher Ni contents have greater resistance to reducing environments, such as exposure to hydrochloric acid, hydrofluoric acid, dilute or intermediate strength sulfuric acid, caustic soda, and dry chlorine. Commercially pure Ni, such as Nickel 270, is often preferred for handling hot concentrated caustic soda, which is a key ingredient in chemical processes, such as paper production and aluminum extraction [1]. MIM superalloys and commercially pure Ni are not commonly available, but they have an untapped market in the chemical processing industry.

EXPERIMENTAL PROCEDURES

One pre-alloyed stainless steel powder, five pre-alloyed superalloy powders, and one carbonyl nickel powder were selected for evaluations. The characteristics of these seven powders are summarized in Table I. They are all -25 μm powders, but there are slight differences in the packing characteristics. SEMs showing the powder morphologies are given in Figure 1. All of the pre-alloyed powders exhibit some satellite formation and a few ligamental particles. Chemical compositions of the superalloy powders are summarized in Table II.

Each powder was mixed with a wax-polymer binder. The pre-alloyed powders were mixed at a solids loading of 65 vol.%, while the carbonyl nickel powder was mixed at 58 vol.%. Test bars were injection molded and debound by a two-step process. First, the components were solvent debound to remove the wax portion of the binder. Then the parts were thermally debound and presintered by heating to 900°C in a hydrogen atmosphere.

The debound and presintered HX bars were sintered at 10°C/minute to temperatures ranging from 1260 to 1300°C. Bars were sintered in both hydrogen and in a 10^{-3} torr vacuum. The debound and presintered 718 bars were sintered at 10°C/min to 1260°C for 1 to 2 hours in a vacuum of 10^{-3} torr. After sintering they were solution heat treated at 980°C for 1 hour in hydrogen and air cooled to room temperature. Then they were aged at 720°C in air for 8 hours, furnace cooled to 620°C, aged in air for 8 hours, and oil quenched. The debound and presintered 625 bars were sintered at 10°C/min to 1290°C for 30 minutes in hydrogen. After sintering the bars were solution heat treated at 1150°C for 2 hours and then oil quenched. The debound and presintered 316L bars were sintered at 10°C/minute to 1330°C for 2 hours in 10^{-3} torr vacuum. The debound and presintered nickel bars were sintered at 10°C/minute to 1350°C for 1 hour in 10^{-3} torr vacuum.

Table I. Powder characteristics

Alloy		316L	HX	HX	718	718	625	270
Vendor		Atmix	Atmix	Osprey	Atmix	Osprey	Atmix	Inco
Pycnometer density (g/cm^3)		7.84	8.14	8.26	8.19	8.20	8.42	8.86
Apparent density (g/cm^3) % of pycnometer		3.03 39%	3.37 41%	3.55 43%	3.33 41%	3.62 44%	3.08 37%	3.71 42%
Tap density (g/cm^3) % of pycnometer		4.18 53%	4.55 56%	4.65 56%	4.66 57%	4.76 58%	5.48 65%	5.26 59%
Particle size (μm)	D_{10}	3.8	4.5	3.2	3.0	3.1	5.1	4.0
	D_{50}	10.2	9.6	7.8	7.4	7.4	9.7	7.1
	D_{90}	21.7	18.4	15.1	15.8	14.5	16.9	11.8

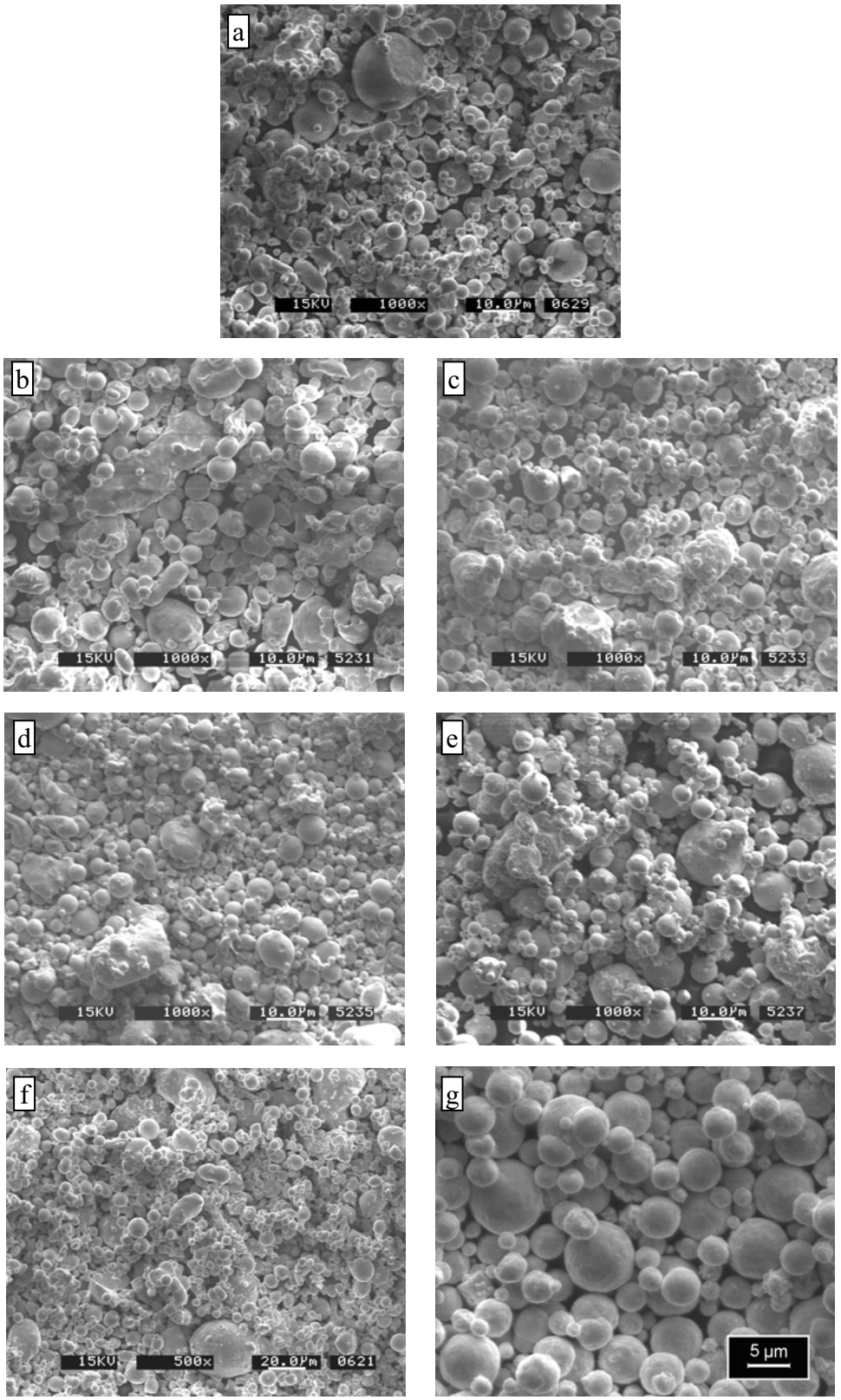

Figure 1. Scanning electron micrographs of the (a) Atmix 316L, (b) Atmix HX, (c) Osprey HX (d) Atmix 718, (e) Osprey 718 (f) Atmix 625, and (g) Inco carbonyl Ni powders.

Table II. Chemical compositions of the superalloy powders.

	Atmix HX	Osprey HX	Atmix 718	Osprey 718	Atmix 625
C	0.095	0.058	0.040	0.046	0.042
Si	0.82	0.77	0.21	0.040	0.33
Mn	0.24	0.46	0.22	0.028	0.34
P	0.018	0.007	0.003	N/M	0.003
S	0.016	0.003	0.003	N/M	0.003
Ni	Balance	Balance	52.62	52.6	Balance
Cr	21.28	21.3	18.93	18.9	21.32
Fe	18.36	18.8	Balance	Balance	1.91
Mo	9.00	9.4	2.99	2.8	9.17
Cu	0.03	0.030	0.00	0.010	N/M
Co	1.49	1.5	0.01	N/M	0.01
Al	N/M	0.016	N/M	0.40	0.11
Ti	N/M	0.005	N/M	0.95	0.01
Nb+Ta	N/M	N/M	5.17	4.9	3.54
W	0.47	0.35	N/M	N/M	N/M
O	0.3160	N/M	0.4500	N/M	0.4600
B	N/M	0.004	N/M	0.006	N/M

N/M = not measured

Sintered densities were determined by Archimedes' technique of water displacement. For metallography, the samples were mounted in Bakelite and polished to a 0.3 μm surface finish. Several chemical and electrochemical reagents were evaluated as etchants. The performance of these etchants varied depending on the processing of the alloys. The vacuum sintered HX samples were chemically etched using 43 vol.% hydrochloric acid, 29 vol.% nitric acid, and 29 vol.% acetic acid. The hydrogen sintered HX samples were electrochemically etched using 33 vol.% sulfuric acid, 33 vol.% nitric acid, and 34 vol.% deionized water. The samples were immersed in the solution for 2 seconds, and an external voltage of 6 volts was applied to them. The 718 samples were electrochemically etched with 25% sulfuric acid and 75% water at 5 volts for 10 seconds. The 625 samples were etched with 25% sulfuric acid and 75% water at 4 volts for 5 seconds.

The tensile strengths of sintered MIM test bars were measured using a MTS Systems Corporation Sintech 20/D universal testing machine with a 20000 lb (88.9 kN) load cell in accordance with MPIF Standard 50. Each sample was measured, placed in the tensile fixture, loaded at 2 mm/minute and monitored for fracture and ultimate tensile loading. Elongation was measured with a set of calipers.

The general corrosion resistance of the MIM alloys to 1M nitric acid, 1M hydrochloric acid, bleach (5.25% sodium hypochlorite solution), 40% sodium hydroxide, and 50% sulfuric acid was measured according to ASTM G 31. Samples for general corrosion testing were immersed for up to 144 hours at ambient temperature. Three test bars for each material and condition were weighed and placed in wide mouth jars. The three bars in each jar were separated from each other and propped against the sidewall of the jar. The test

bars were completely immersed with 175 mL of the corrosive media. The jar was covered and the parts were allowed to sit without aeration. After the set duration the parts were removed, rinsed, scrubbed with a bristle brush, and ultrasonically cleaned in distilled water to remove the corrosion products. The samples were placed in a 60°C drying oven for 1 hour and then weighed to determine the mass loss. The corrosion rate R in mils per year (mpy) was calculated based on the surface area A (in cm^2) of the test bars and the density D (in g/cm^3) of the material using the formula

$$R = \frac{3.45 \cdot 10^6 M}{ATD} \quad (1)$$

where M is the mass loss (in g) and T is the time of exposure (in hours). Scanning electron microscopy (backscatter) was used for examination of the corrosion-tested surfaces.

RESULTS AND DISCUSSION

Alloy HX

The sintered densities achieved with the HX test bars are summarized in Table III for several sintering conditions. Both powders resulted in similar densities. The highest sintered density was achieved in vacuum at 1275°C, but was only 94.5% of the wrought density (8.14 g/cm^3).

Microstructures of the Osprey powder samples sintered at 1275°C and at 1300°C are shown in Figure 2. At 1275°C, large grains are seen in Figure 5(a) with many of the pores separated from the grain boundaries. At 1300°C, the grains are even larger with no decrease in porosity. Densification occurred solely by solid-state sintering with no liquid forming below 1335°C as determined by differential thermal analysis (DTA) of the powders. Based on this result and the micrographs, pore-grain boundary separation takes place at the on-set of the final stage of solid-state sintering, inhibiting further densification.

The sintered densities are lower than those reported by researchers at Allied Signal/Honeywell [2,3], who reported a density of 99% for MIM HX using a 20 μm powder. Sintering was performed at 1260°C, after pulling a vacuum and backfilling the furnace with hydrogen. Further processing details were lacking. The starting powder chemistry may affect liquid phase formation.

Table III. Sintered densities of HX test bars.

Sintering conditions	Atmix sintered density		Osprey sintered density	
	g/cm^3	% of wrought	g/cm^3	% of wrought
1260°C, 2 hrs, 10^{-3} torr	7.58	93.1%	7.52	92.4%
1260°C, 2 hrs, hydrogen	7.27	89.3%	7.21	88.6%
1275°C, 1 hr, 10^{-3} torr	7.69	94.5%	7.61	93.5%
1300°C, 1 hr, hydrogen	7.52	92.4%	7.64	93.9%

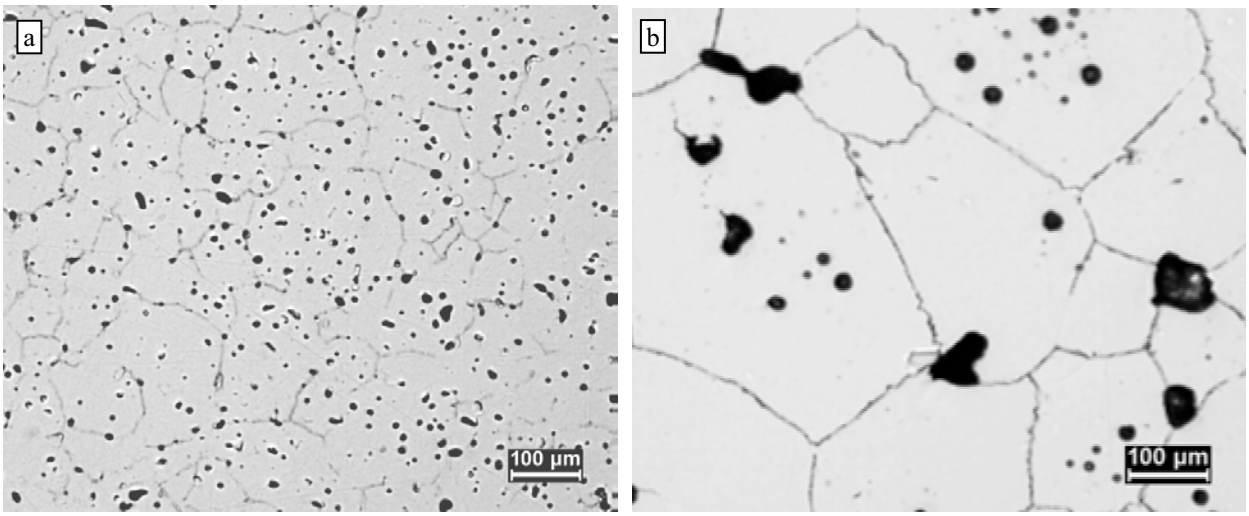

Figure 2. Optical micrographs of etched MIM HX test bars produced from the Osprey powder and sintered at (a) 1275°C for 1 hour in vacuum and (b) 1300°C for 1 hour in hydrogen.

Alloy 718

The sintered densities of the 718 bars after sintering for 1260°C in a vacuum of 10^{-3} torr are given in Table IV. Both powders sintered to high densities. The sintering temperature was at the handbook value [4] for the solidus, so densification may be slightly enhanced by super-solidus liquid phase sintering. Some improvement in density was achieved by increasing the hold time from 1 to 2 hours.

Electrochemical etching after aging at 720°C reveals precipitates along the grain boundaries as shown in Figure 3. The micrographs show very few γ″ precipitates along the grain boundaries, suggesting incomplete aging. The γ″ precipitates have platelet morphology, while the spherical precipitates may be γ′. After the second aging cycle at 620°C, more precipitates form as shown in Figure 4, which reveals γ″, γ′, and possibly some globular MC type carbide precipitates. The grain size is estimated to be between 10 and 15 µm.

Table IV. Sintered densities of 718 test bars

Sintering conditions	Atmix sintered density		Osprey sintered density	
	g/cm^3	% of wrought	g/cm^3	% of wrought
1260°C, 1 hrs, 10^{-3} torr	7.92	96.7%	7.92	96.7%
1260°C, 2 hrs, 10^{-3} torr	8.09	98.8%	8.06	98.4%

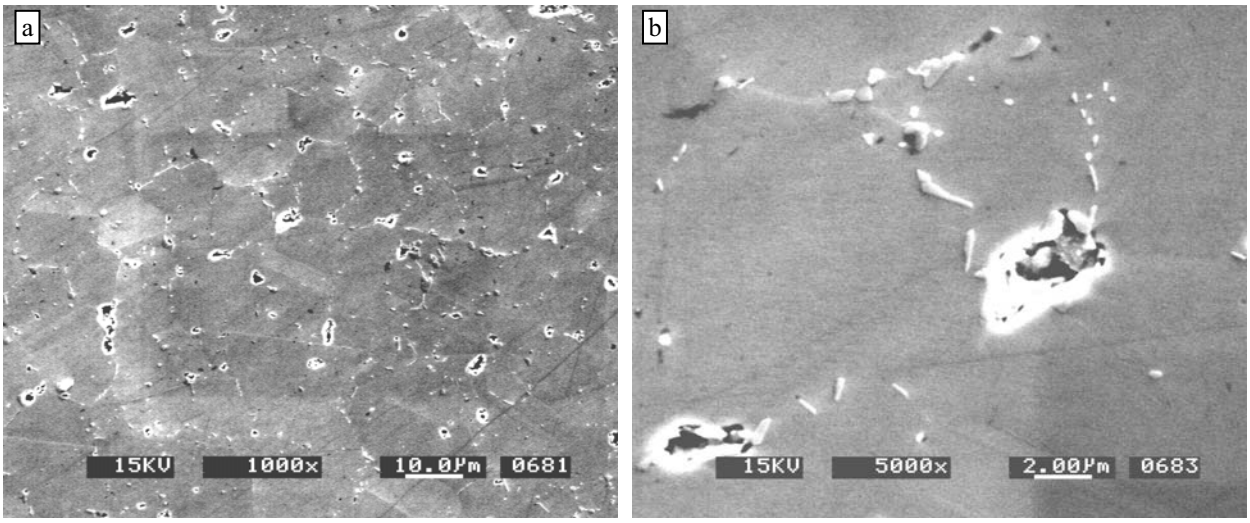

Figure 3. SEM micrographs of electrolytically etched MIM 718 test bars produced from the Osprey powder sintered at 1260°C for 1 hour in vacuum, solutionized, aged at 720°C for 8 hours, and air cooled.

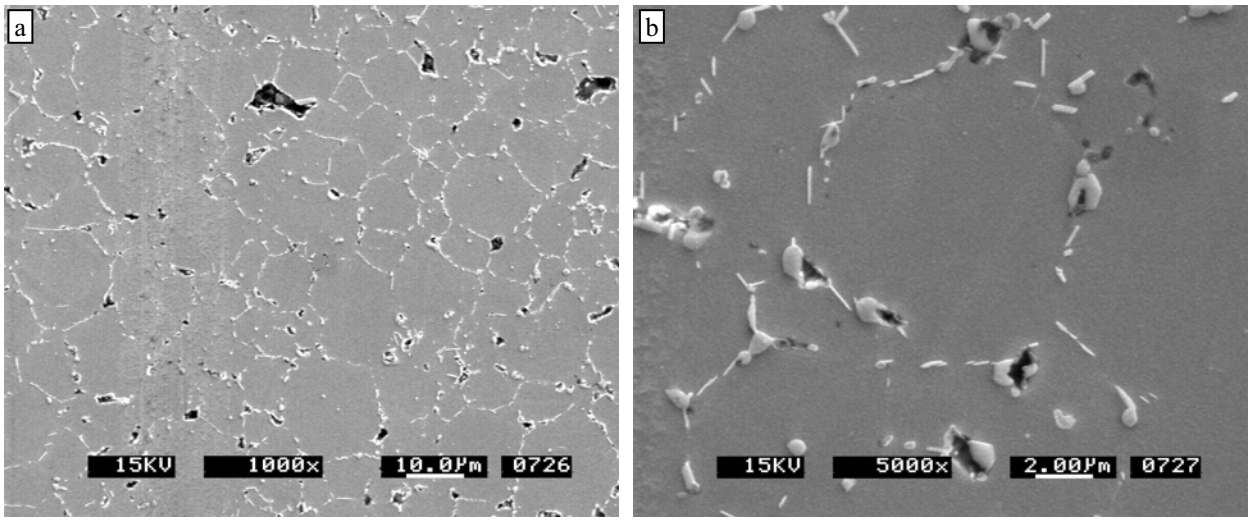

Figure 4. SEM micrographs of electrolytically etched MIM 718 test bars produced from the Osprey powder sintered at 1260°C for 1 hour in vacuum and heat treated.

The mechanical properties are summarized in Table V. The yield and ultimate tensile strengths were comparable to cast properties, but were below expectations for wrought material. The ductility was low, even in comparison to cast material.

The as-sintered densities of the present study fall within the ranges reported by an effort led by Pratt and Whitney [5-8]. Using an 8.5 µm 718 powder, densities of 94 to nearly 100% of theoretical were achieved after vacuum sintering with Ar partial pressure of 10^{-3} to 10^{-4} torr at temperatures ranging from 1250°C to 1275°C for 2 to 8 hours. Ultimate tensile strengths of 812 to 1218 MPa and yield strengths of 686 to 995 MPa were obtained [6]. Elongations ranged from 3.3 to 17.4%. Subsequent hot isostatic pressing at 1190°C and 1020 atm for 4 hours gave full density and mechanical properties just slightly below AMS 5596 criteria for wrought material [8].

Table V. Comparison of the properties of heat treated MIM 718 produced from the Atmix powder to typical properties of cast and wrought material [4].

	MIM 1260°C, 2 hrs	Typical Wrought	Typical Cast
Density (g/cm^3)	8.09 (98.8%)	8.19	-
YS (MPa)	900	1185	915
UTS (MPa)	1065	1435	1090
Elongation	4%	21%	11%
Hardness	31-33 HRC	36 HRC	-

Alloy 625

The sintered densities and mechanical properties of the 625 bars after sintering at 1290°C in hydrogen are given in Table VI. An optical micrograph of the heat treated material is shown in Figure 5. The average grain size is approximately 90 µm. The handbook value [4] for the solidus is 1290°C, but the sintering temperature appears to be just above the solidus, allowing rapid densification via supersolidus liquid phase sintering, but also giving significant grain coarsening. The mechanical properties are below those typical of both wrought and cast material. Further optimization of the sintering parameters is needed.

Mechanical properties of 625 were also reported by the effort led by Pratt and Whitney [4,5]. Using an 8.5 µm 625 powder densities above 99% of theoretical were achieved by sintering in hydrogen in the temperature range of 1288 to 1298°C for 24 to 60 minutes. Optimization of the sintering time and temperature to maximize density while maintaining a fine grain size resulted in mechanical properties comparable or better than those of cast and solution treated material [5].

Table VI. Comparison of the properties of heat treated MIM 625 to typical properties of cast and wrought material [4].

	MIM 1290°C, 0.5 hr	Typical Wrought	Typical Cast
Density (g/cm^3)	8.40 (99.5%)	8.44	-
YS (MPa)	230	490	350
UTS (MPa)	600	965	710
Elongation	21%	50%	58%
Hardness	91 HRB	91.5 HB	-

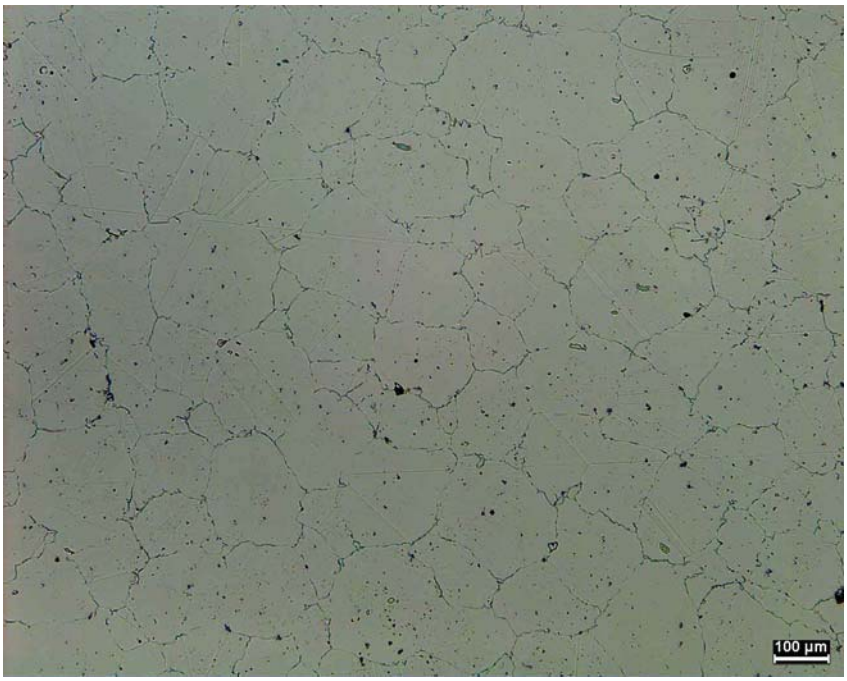

Figure 5. Optical micrograph of etched MIM 625 test bars produced from the Atmix powder, sintered at 1290°C for 1 hour in hydrogen and solution heat treated.

Corrosion Resistance

Corrosion studies on MIM alloys have generally focused on stainless steels, including 316L, 17-4 PH, JP51, 420, and 440C [9-13]. MIM superalloys have been less thoroughly evaluated. The previously referenced studies [2-7] focused on the mechanical properties, although Ni-based superalloys also have excellent corrosion properties. In this study, the MIM HX, 718, and 625 test bars were subjected to corrosion testing along with MIM 316L austenitic stainless steel and MIM 270 commercially pure nickel. Processing details on the MIM 316L and MIM 270 are given in a previous paper [14]. The sintered densities of the 316L and 270 were 94.6% and 95.2%, respectively. Prior to testing, backscatter SEMs of the as-sintered surfaces of the five compositions were taken and are shown in Figure 6. The 316L and 270 samples show similar levels of surface texture and surface porosity. The 718 sample shows a more textured surface. A porous surface is seen in the HX sample due to its relatively low sintered density.

The corrosion resistance of the MIM superalloys is compared to that of MIM 316L and MIM 270 in Table VII. The oxidizing media – nitric acid and bleach – attacked 270 much more severely than 316L or the superalloys as expected. On the other hand, 270 had significantly better performance over 316L and 718 in the reducing sulfuric acid. The 718 was also more susceptible to attack by hydrochloric acid, which is also reducing. The 625 showed excellent corrosion resistance to both oxidizing and reducing media. HX had relatively good corrosion resistance to both hydrochloric acid and sulfuric acid despite its higher porosity.

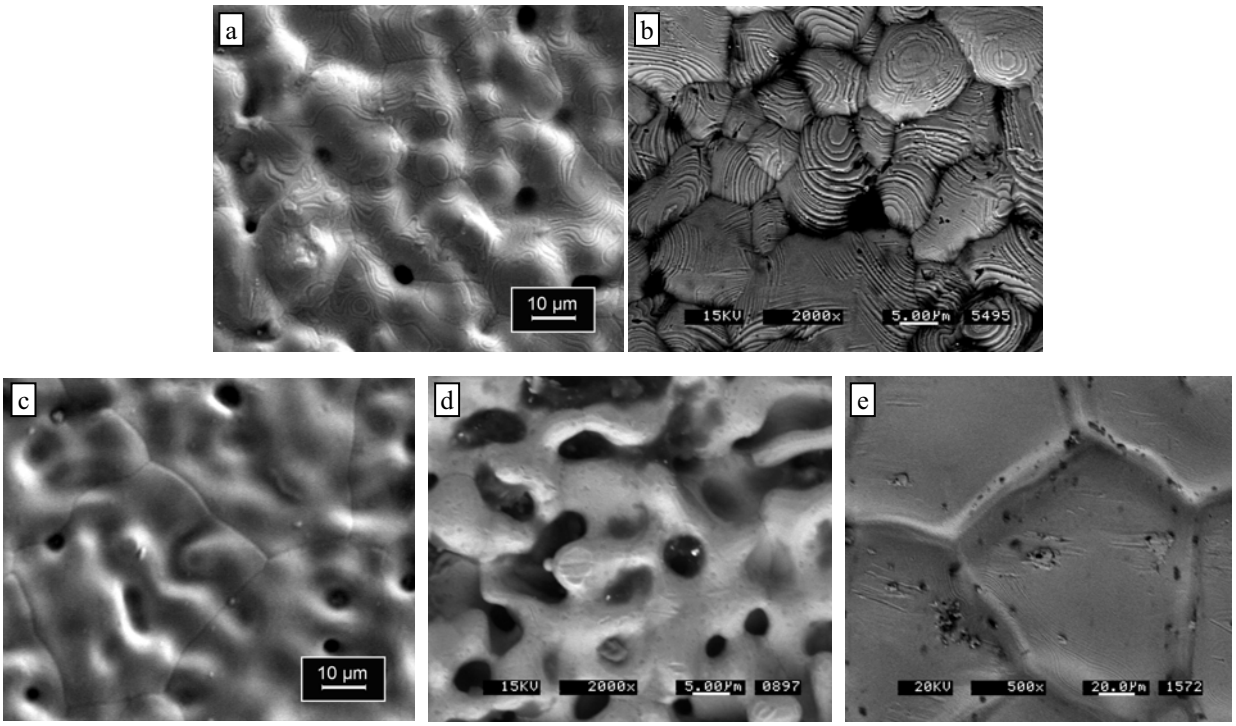

Figure 6. Backscatter SEMs of the sintered surfaces of (a) 316L, (b) 718, (c) 270, (d) HX, and (e) 625.

Table VII. Corrosion rates for the various alloys

Corrosive media	316L mpy	HX mpy	718 mpy	625 mpy	270 mpy
Nitric acid	0.0	-	0.0	0.0	160
Hydrochloric acid	8.8	3.8	16	0.3	5.5
Bleach	0.0	-	0.1	0.1	79
Sodium hydroxide	0.8	-	0.0	0.0	0.0
Sulfuric acid	36	1.7	42	0.0	0.3

Backscatter SEMs of the 316L, 718, and 270 samples after immersion in sulfuric acid are given in Figure 7. The 270 sample shows only slight general attack with intact grain boundaries and little change to the surface pore morphology. The 316L sample shows significant general attack and a smearing of the grains and pores. The 718 sample shows preferential etching along specific crystallographic orientations.

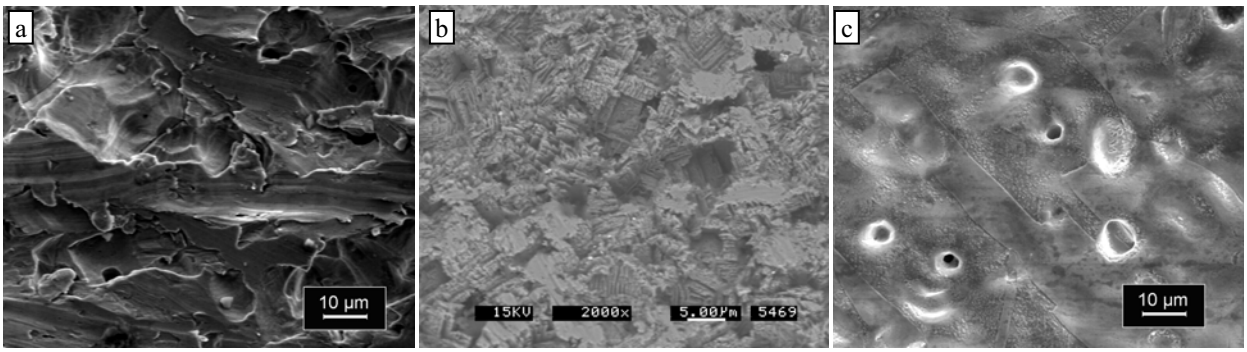

Figure 7. Backscatter SEMs of the surfaces of (a) 316L, (b) 718, and (c) 270 after corrosion testing in H_2SO_4.

At room temperature, 270 performed only slightly better than 316L in hydrochloric acid and the 718 was severely attacked. Backscatter SEMs of these samples after immersion in hydrochloric acid are given in Figure 8. The 270 sample shows general corrosion as evidenced by attack along preferential planes. The 316L sample also shows general corrosion, but mostly dealloying and etch pitting. The 718 shows significant general corrosion.

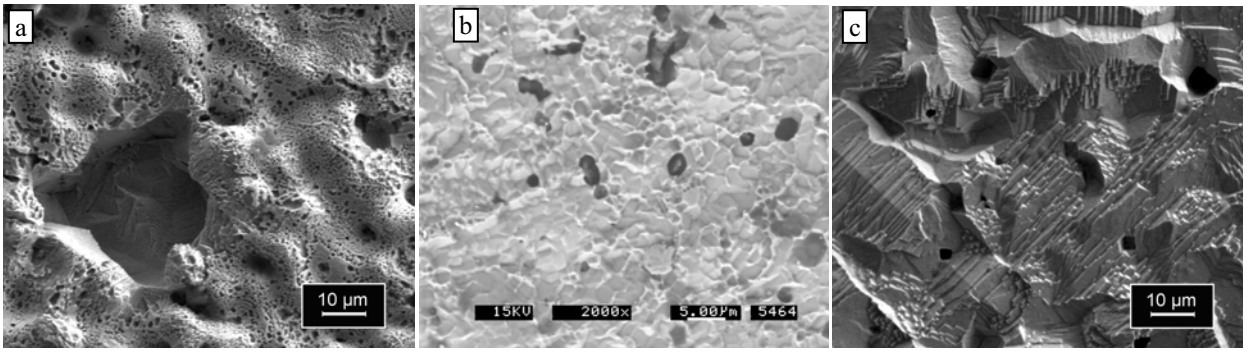

Figure 8. Backscatter SEMs of the surfaces of (a) 316L and (b) 718 and (c) 270 after corrosion testing in HCl.

The 316L results from the present study correlate favorably with the results from Collins [13], who tested six MIM 316L stainless steels, which gave a range of corrosion rates for different media. All six performed well in nitric acid and the range was only 0 to 0.9 mpy (0 to 0.02 mm/year). A much wider range, 0.2 to 116 mpy (0.005 to 2.9 mm/year), was observed for the samples immersed in bleach. Hydrochloric acid gave a range from 3.2 to 43 mpy (0.08 to 1.1 mm/year). Some of these tested samples showed significant attack of the grain boundaries, which was not seen for the 316L sample in the present work. Still, MIM stainless steels generally perform as well as wrought materials in general corrosion tests.

Since the 270 samples contain no second phases and have low levels of impurities, corrosion occurs primarily by general surface attack as seen in the backscatter SEM of the sample tested in HCl. The 270 corrosion rate of 5.5 mpy (0.1 mm/year) in hydrochloric acid is in line with handbook values [1] for commercially pure nickel. The lack of corrosion in sodium hydroxide is also expected. At temperatures below 100°C, the corrosion rate of nickel in sodium hydroxide is less than 1 mpy (0.03 mm/year). With

low impurities, nickel retains good corrosion resistance against sodium hydroxide to temperatures over 315°C. At these temperatures 316L is readily attacked. Concentrations of sulfuric acid up to about 60% are considered non-oxidizing and give high corrosion rates for 316L by breaking down its oxide layer. Commercially pure nickel has generally good corrosion resistance to these concentrations of sulfuric acid, as confirmed by the MIM 270 samples.

The Ni-Cr superalloys, especially 625 perform well in all three types – neutral, oxidizing, and reducing – of aqueous environments. The 718 performed like 316L in the oxidizing nitric acid and like 270 in the reducing sodium hydroxide. However, it performed worse than both 316L and 270 in hydrochloric and sulfuric acids. Alloy 625, which contains less iron, is generally recommended for applications involving these corrosive media.

CONCLUSIONS

Achieving high densities with 718 and 625 requires sintering at or just above the solidus temperature. For the HX powders investigated in this study, sintered densities are limited by the lack of a liquid phase up to a temperature at which pore-grain boundary separation occurs. Powder chemistry is a key factor affecting liquid phase formation and the processing window for sintering to high density and optimal mechanical properties.

MIM can produce alloys with a range of Ni contents to tailor corrosion properties for specific applications. MIM 316L has good corrosion resistance to oxidizing environments such as nitric acid and bleach, but MIM 270 is better suited to reducing environments such as sodium hydroxide and dilute solutions of sulfuric acid. MIM 718 is suitable for both oxidizing media such as nitric acid and reducing media such as sodium hydroxide, but performs poorly in hydrochloric acid and sulfuric acid where MIM HX performs better. MIM 625 has excellent resistance to all of these corrosive media.

ACKNOWLEDGEMENTS

The authors gratefully acknowledge Gaurav Aggrawal, Ravi Bollina, Ethan Westcot, Derek Schoiack, Ben Smarslok, and Chee Hoo Liang for their assistance with the experiments and testing performed during this research study.

REFERENCES

[1] Mankins, W.L. and Lamb, S., *ASM Metals Handbook, Vol. 2, Properties and Selection: Nonferrous Alloys and Special-Purpose Materials*, 1990, p. 428.
[2] LaSalle, J.C., Sherman, B., Scott, C., Bartone, K., Bellows, R., and Lowery, D., "Aircraft Engine Combustor Swirlers Fabricated Using Aqueous Based Binder Metal Injection Molding," *Advances in Powder Metallurgy & Particulate Materials - 1999*, compiled by C.L. Rose and M.H. Thibodeau, MPIF, Princeton, NJ, 1999, pp. 6.39-6.44.
[3] Holmes, B., Hatfield, P., and Sherman, B., "Dimensional Predictability and Consistency in Aircraft Engine Components when Molding with an Aqueous Based Binder System," *Advances in Powder Metallurgy and Particulate Materials – 1999,* compiled by C.L. Rose and M.H. Thibodeau, MPIF, Princeton, NJ, 1999, pp. 6.82- 6.88.
[4] *ASM Specialty Handbook: Nickel, Cobalt, and Their Alloys*, compiled by J.R. Davis, ASM International, Materials Park, OH, 2000.
[5] Hens, K.F., Grohowski, J.A., German, R.M., Valencia, J.J, and McCabe, T., "Processing of Superalloys via Powder Injection Molding," *Advances in Powder Metallurgy & Particulate Materials – 1994*, vol. 4, compiled by C. Lall and A.J. Neupaver, MPIF, Princeton, NJ, 1994, pp. 137-149.

[6] Valencia, J.J., McCabe, T., Hens, K., Hansen, J.O, and Bose, A., "Microstructure and Mechanical Properties of Inconel 625 and 718 Alloys Processed by Powder Injection Molding," *Conference on Superalloys 718, 625, 706, and Various Derivatives*, compiled by E.A. Loria , TMS, Pittsburgh, PA, June 26-29, 1994, pp. 935-45.
[7] Bose, A., Schmees, R., Valencia, J.J., and Spirko, J., Powder Injection Molding of Inconel 718," *Advances in Powder Metallurgy and Particulate Materials – 1997*, compiled by R.A. McKotch and R. Webb, MPIF, Princeton, NJ, 1997, pp. 18.99-18.112.
[8] Schmees, R.M., and Valencia, J.J., "Mechanical Properties of Powder Injection Molded Inconel 718," *Advances in Powder Metallurgy and Particulate Materials – 1998,* compiled by J.J. Oakes and J.H Reinshagen, MPIF, Princeton, NJ, 1998, pp. 5.107-5.118.
[9] Wohlfromm, H., Blömacher, M., Weinand, D., Uggowitzer, P.J., and Spediel, M.O., *Proceedings of the 1998 PM World Congress*, Granada, Spain, published on CD by the European Powder Metallurgy Association, 1998.
[10] Wohlfromm, H., Blömacher, M., Uggowitzer, P.J., Magdowski, R., and Spediel M.O., *Advances in Powder Metallurgy and Particulate Materials – 1999*, vol. 2, compiled by C.L. Rose and M.H. Thibodeau, MPIF, Princeton, NJ, 1999, pp. 6-27-6.38.
[11] Tandon, R., Simmons, J.W., Covino, B.S., and Russel, J.H., *Inter. J. of Powder Metall.*, vol. 34, no. 8, 1998, pp. 47-54.
[12] Bulger, M.K. and Erickson, A.R., *Advances in Powder Metallurgy and Particulate Materials – 1994*, vol. 4, compiled by C. Lall and A.J. Neupaver, MPIF, Princeton, NJ, 1994, pp. 197-215.
[13] Collins, S.R., *Advances in Powder Metallurgy and Particulate Materials - 2002*, vol. 3, compiled by V. Arnhold, C. Chu, W.F. Jandeska, Jr., and H.I. Sanderow, MPIF, Princeton, NJ, 2002, pp. 10.240-10.254.
[14] Johnson, J.L. and Westcot, E.J. "Metal Injection Molding of Commercially Pure Nickel for the Chemical Processing Industry," *Inter. J. of Powder. Metal.*, vol. 39, no. 8, 2003, pp. 37-45.